Structural characterisation of Magnesium (Sodium) Aluminium Silicate Hydrate (M-(N)-A-S-H) phases by X-ray absorption near-edge spectroscopy

Marika Vespa[a*], Camelia Borca[b], Thomas Huthwelker[b], Barbara Lothenbach[c], Rainer Dähn[d], Erich Wieland [d*],

[a] Geochemical and Environmental Consulting (GeochEnv Consulting) 79737 Herrischried, Germany

[b] Paul Scherrer Institute, Swiss Light Source, 5232 Villigen PSI, Switzerland

[c] Empa, Laboratory for Concrete & Construction Chemistry, Überlandstrasse 129, 8600 Dübendorf, Switzerland

[d] Paul Scherrer Institute, Laboratory for Waste Management, 5232 Villigen PSI, Switzerland

For submission to Applied Geochemistry

Key words. Synchrotron-based XAS, near-edge X-ray absorption fine structure NEXAFS, Mg-Al silicate hydrates M-A-S-H, Mg sodium aluminium silicate hydrate M-N-A-S-H

*Corresponding author, present address:

Marika Vespa

Brenk Systemplanung

Heider-Hof-Weg 23, D-52080 Aachen, Germany

Phone: +49 2404 4651 47

E-mail: m.vespa@brenk.com

Abstract

Magnesium silicate hydrate phases (M-S-H) have recently been observed forming in low pH cements, which came in contact with Mg-rich ground waters or argillaceous rock formations, such as Opalinus Clay. Their crystallographic structure has been suggested to be a purely ordered sheet-like phyllosilicate with a tetrahedral octahedral tetrahedral octahedral (TOT O) layering, i.e. similarly to a talc plus brucite structure. In nature, Mg phyllosilicate with this type of layering contain several type of cations, in particular Al, as well as alkaline earth metals. This study shows that the X-ray near-edge spectra of synthesised Mg/Al- silicate hydrates and Mg/Al/Na silicate hydrates (M-A-S-H and M-N-A-S-H) show distinct differences to M-S-H, indicating the possible accommodation of Al in its structure. This is further supported by the great similarity of the spectra to natural Mg-Al containing phyllosilicate, i.e. clinochlore, having a TOT O layering. The results, furthermore, suggest that Na is not taken up in the structure due to the strong similarities of the M-N-A-S-H with the M-A-S-H phases. The comparison of the latter spectra with natural references show high resemblance not only with clinochlore, but also with sepiolite, a Mg containing phyllosilicate with water molecules bridging between broken octahedral chains. It is, therefore, suggested that the Mg in the M-(N)-A-S-H phases is bound similarly to clinochlore with a TOT O layering and that water molecules or OH groups are present between broken octahedral layers. Aluminium is possibly accommodated in the tetrahedral and / or octahedral layers.

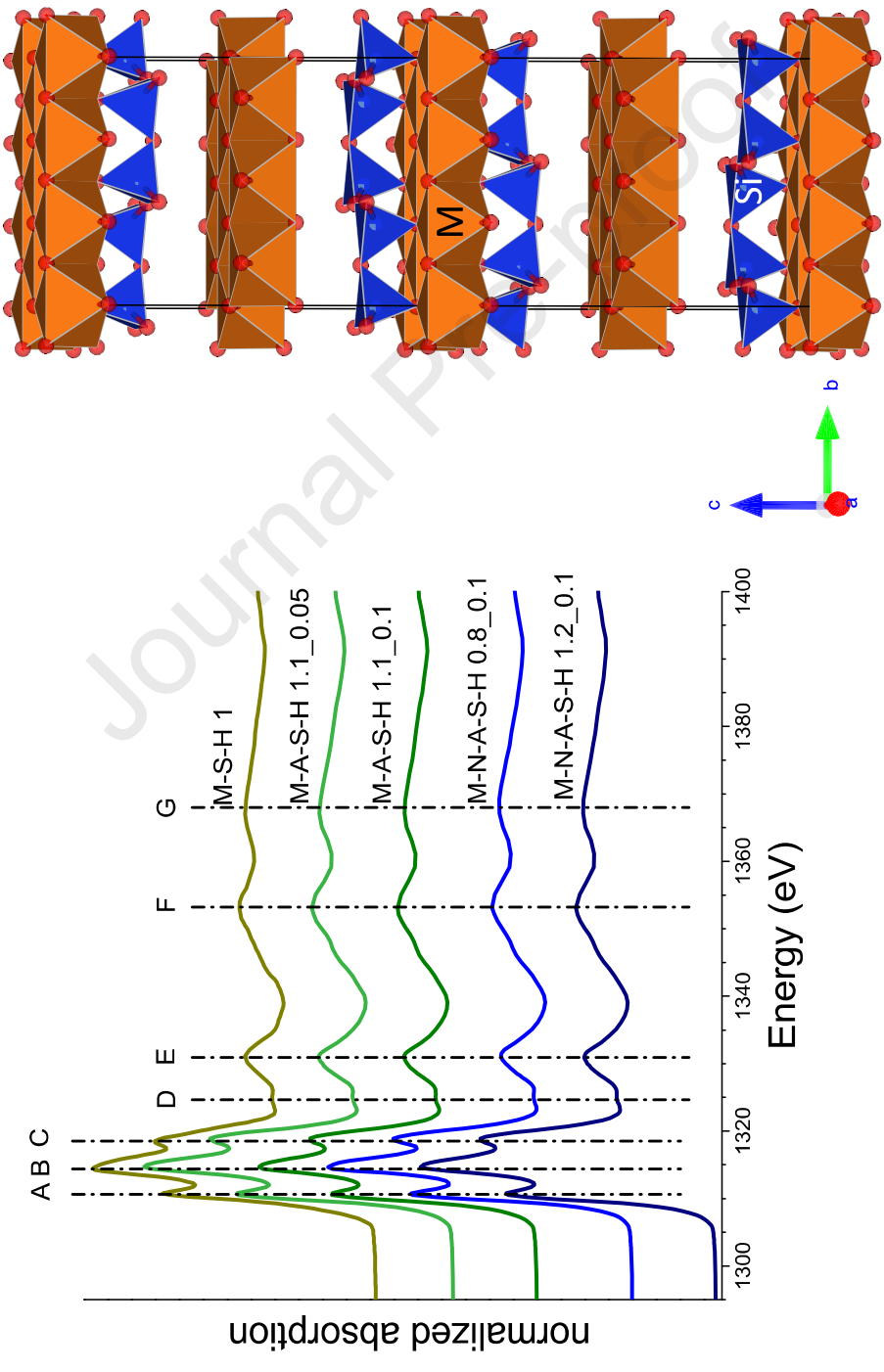

1. Introduction

The significance of Magnesium Silicate Hydrate (M-S-H) phases is continuously growing, both within the context of durability of concrete and of waste management, since M-S-H are expected to form in cement contacting with argillaceous rock formations, which are foreseen in many countries as host rock for radioactive waste disposal and, during the course of the hydration of alternative binder materials with a high MgO content (Brew and Glasser, 2005). Indeed former investigations show that at the contact interface between various cements and clays, specifically the Opalinus clay (OPA), massive Mg accumulation occurs (Dauzères et al., 2016; Jenni et al., 2014; Mäder et al., 2017). The contact between cement and OPA and the evolution of the contact zone with time is an issue of concern in the concept of the Swiss deep geological repository for radioactive waste. For example, spent fuel and high- level radioactive waste are planned to be disposed of in the OPA in which liners made of low-pH cement are intended to reinforce the engineer barrier system.

Recent X-ray absorption spectroscopic data indicate the possible formation of poorly crystalline M-S-H (Vespa et al., 2018). A detailed wet chemistry and NMR study (Bernard et al., 2020a) showed the incorporation of aluminum in M-S-H up to Al/Si ~ 0.2 in both octahedral and tetrahedral layers. Magnesium, calcium and alkali ions, if present, can be bound to the cation exchange sites of M-S-H compensating its negative surface charge (Bernard et al., 2018a; Bernard et al., 2019), while no Al was found to be present on the cation exchange sites. M-S-H phases have a sheet-like structure similar to trioctahedral phyllosilicates and in particular to talc (Bernard et al., 2020a; Vespa et al., 2017). Nonetheless, these phases are not well ordered. Talc is composed of Mg octahedra sandwiched between sheets of silica tetrahedra and OH groups sitting in the plane of the bridging oxygens between the octahedra and tetrahedra. Although, the M-S-H phases show similarities to talc, ^{29}Si-NMR data (Nied et al., 2016) and XRD analysis (Roosz et al., 2015) indicate clear differences. The broad XRD reflections and the presence of $^{1}/_{3}$ of Q^2 Si sites

and some Q^1 (end of chain silica) reflect a disordered structure with vacancies or broken chains in the sheet silicate network and/or very small coherent silica regions. In addition, a high amount of hydroxyl groups probably bound to the octahedral MgO sheet and of loosely associated water was observed for synthetic M-S-H with the following chemical formula $Mg_3Si_4O_{10}(OH)_2$ $4H_2O$ (Nied et al., 2016). This is a quite different structure compared to Calcium Silicate Hydrate (C-S-H) phase. The latter has a layered structure with seven-fold coordinated Ca and tetrahedral Si based on single silica chains (Richardson, 2008). Nevertheless, the formation of mixed Mg Ca Silicate Hydrate (M-C-S-H) phases have been suggested by various authors (Fernandez et al., 2008; Pytel and Malolepszy, 2000; Shrivastava et al., 1991), while others have reported the co-existence of the two distinct M-S-H and C-S-H phases (Bernard et al., 2017; Lothenbach et al., 2015). Whether Ca is present in the M-S-H structure was impossible to be determined by standard laboratory analytical bulk methods. Recent wet chemistry investigations of samples containing both Ca and Mg (Bernard et al., 2018b) indicate the incorporation up to 5 mol.% of Ca in the M-S-H structure. Also XANES spectroscopic analysis combined with ab initio calculation showed that Ca may be incorporated in the M-S-H structure (Vespa et al., 2018). However, in nature, Mg-rich phyllosilicates tend to incorporate Al rather than Ca. Thus, the formation of Mg Al Silicate Hydrate (M-A-S-H) phases is expected.

This study aims at characterising the M-S-H structure and to unequivocally verify the possibility of Al incorporation into the M-S-H structure by using synchrotron-based X-ray absorption near edge spectroscopy (XANES). XANES is mainly used to discern the oxidation state of the X-ray absorber, based on the edge position, and for fingerprinting by comparing experimental spectra of unknown species with reference compounds. The characterisation and knowledge of the structure of M-S-H phases and the knowledge of Al incorporation in the structure will be essential for identifying the Mg-rich phases at the cement/OPA interfaces and other clay formations. Furthermore, structural information on M-S-H/M-A-S-H/M-C-S-H

phases is important with the aim of developing thermodynamic models used to predict the long-term interaction of cements with clay formations in the framework of performance assessments of deep geological repositories.

2. Materials and Methods

2.1. Sample preparation

Magnesium oxide (Merck, pro analysis) and silica fume (SiO_2, Aerosil 200, Degussa-Huls, Switzerland) were chosen as starting materials for the M-A-S-H synthesis as detailed elsewhere (Bernard et al., 2020a). In a first series, metakaolin ($Al_2O_3.2SiO_2$, ARGICAL-M 1200S, IMERYS, France; purity 93.8) was used as a source of aluminum. The starting mixes of these so-called M-A-S-H were prepared with Mg/Si=1.1 and Al/Si ratio of 0.05 and 0.10. The Al was incorporated in both the octahedral and tetrahedral main layers of M-A-S-H; its final composition corresponded to Mg/Si=1.1 and Al/Si of 0.05 and 0.10 (Bernard et al., 2020a). The samples are labelled accordingly: M-A-S-H 1.1_0.05 and M-A-S-H 1.1_0.1

A second series was prepared using sodium aluminate ($NaAlO_2$, anhydrous, technical from Sigma Aldrich), nitric acid (HNO_3, Merck, suprapur, 65%), and sodium nitrate ($NaNO_3$, VWR chemicals, Analar normapur) for the synthesis of M-A-S-H in presence of sodium targeting a pH < 11.5. Two Mg/Si ratios were studied: 0.8 and 1.2 while the Al/Si ratios in the mixes was set to 0.10 (Bernard et al., 2020a). The final M-A-S-H contained less than the targeted Al/Si of 0.1, as approximately 20% of the Al were bound in hydrotalcite and a zeolitic phase, which limited the Al-uptake into M-(A-)S-H compared to systems without sodium nitrate (Bernard et al., 2020b). The samples are labelled M-N-A-S-H 0.8_0.1 and M-N-A-S-H 1.2_0.1.

The samples were prepared in polyethylene (PE-HD) containers using ultrapure water (18.2 MΩ.cm resistance) generated by a Milli-Q Gradient A10 purification system (Millipore, USA) and a water/solid (W/S) ratio of 45 to ensure a homogeneous suspension as described in detail in (Bernard et al., 2020a). Sample preparation was carried out in a glove box under N_2 to avoid CO_2 contamination. The samples were equilibrated at 20°C and placed on a horizontal shaker.

The first series with the metakaolin addition had some residual quartz (SiO_2) and anatase (TiO_2), whereas the second series (with $NaAlO_2$ and $NaNO_3$) contained only some unreacted silica and polycondensated aluminosilicates (an amorphous zeolitic precursor); in addition some NO_3-hydrotalcite could have been present as detailed in (Bernard et al., 2020a). Note that these residual phases with the exception of NO_3-hydrotalcite are not detectable by the Mg K-edge XANES, since they are not associated with the Mg atoms.

Given the strong similarities between the M-S-H 1 and 0.8 and the fact that in this study Mg/Si ratios of 0.8, 1.1 and 1.2 were investigated, the pure magnesium silicate hydrate (M-S-H 1) (Lothenbach et al., 2015; Vespa et al., 2018) with a Mg/Si=1 ratio was chosen as reference material together with further natural minerals (Table 1).

2.2. XANES data collection and reduction

All XANES spectra at the Mg K-edge were collected at the PHOENIX (**PHO**tons for the **E**xploration of **N**ature by **I**maging and **X**AFS) beamline at the Swiss Light Source (SLS) of the Paul Scherrer Institute (PSI) in Switzerland. The PHOENIX beamline, consisting of PHOENIX I and II branches, uses an elliptical undulator as photon source. The PHOENIX I branch employs a double crystal monochromator. The optics of this branch closely follows the optical concept of the former LUCIA beamline (Flank et al., 2006), which is

158 now located at the Soleil synchrotron in France. The energy range from 0.8 to 8 keV can
159 be covered depending on the choice of crystals. For this work we have used the
160 $KTiOPO_4$(011) crystal pair. Suppression of high order light is achieved by a double
161 reflection on two co-planar mirrors upstream of the monochromator. The PHOENIX II
162 endstation is located at the exit of the X-Treme beamline (Piamonteze et al., 2012). Both
163 the PHOENIX I and the X-Treme beamline share the same undulator as photon source.
164 The X-Treme beamline uses a planar grating monochromator. The rejection of high
165 harmonics is made by appropriate choice of the scattering angles between grating and
166 mirror in the monochromator. The measurements were conducted at room temperature
167 in vacuum ($\sim 10^{-5}$ mbar) with a 1 mm beam size and a beam resolution of 0.16 eV in the
168 energy range of 1200 up to 1500 eV. The step sizes of 5, 0.3, 1, 2 and 5 were used for five
169 scanning regions with energies up to 1300, 1330, 1350, 1400, 1500 eV, respectively.
170 Two detection modes were employed: Total Electron Yield (TEY) and X-ray
171 fluorescence. X-ray fluorescence was recorded using a 4-element Vortex detector. The
172 four detector elements are covered with a thin ($\sim$5 μm) plastic foil. Simultaneously, the
173 TEY signal was recorded by measuring the total current into the sample. Note that the
174 sample was mounted electrically insulated from the experimental chamber. The
175 intensity of the incoming beam, I_0, was recorded using the TEY signal collected by a Ni
176 coated polyester foil. The monochromator was calibrated to the first inflection point of
177 the K-edge absorption spectrum of Al metal foil.
178 All natural minerals and experimental phases were finely ground. A thin powder layer
179 was spread onto a thin indium foil attached onto the copper plate, which served as
180 sample holder for the measurements.
181 The XANES spectra were extracted from raw data with the Athena interface of the
182 IFFEFIT software (Newville, 2001; Ravel and Newville, 2005). The fluorescence signal

was checked for self-absorption by comparison with spectra taken with the TEY and corrected accordingly. The fluorescence signal was chosen due to the significantly better signal / noise ratio. Linear combination fits were performed using the Athena interface of the IFFEFIT software (Newville, 2001; Ravel and Newville, 2005).

3. Results

3.1 . Characterisation of Magnesium (Sodium) Aluminum Silicate Hydrate phases

3.1.1. Comparison with the Magnesium-Silicate-Hydrate phase

Both the M-A-S-H and M-N-A-S-H XANES spectra showed similarities to the M-S-H 1 spectrum (Fig. 1a), e.g. the typical three peaks near the edge (A, B, C) followed by the oscillations D, E, F and G (Vespa et al., 2018). The energy position, the shape and absorption intensities of these peaks are all comparable. Nevertheless, peak B for both M-A-S-H and M-N-A-S-H spectra showed a slight shift to higher energies compared to the M-S-H (Fig. 1a). Peak A, B and C showed higher absorption intensities for all phases except for the M-A-S-H 1.1_0.1 phase (Fig. 1b). Peaks F and G also showed slightly higher absorption intensities compared to the M-S-H 1, especially for the M-A-S-H 1.1_0.05, whereas for peak D a lower intensity for all M-(N)-A-S-H as for the M-S-H 1 was observed (Fig. 1b and c).

Similarities were also observed between the M-N-A-S-H and the M-A-S-H phases. Nevertheless, some differences appeared in the spectra (Fig. 1d). Peaks A, B and C showed small differences in the absorption intensities between the M-N-A-S-H and M-A-S-H spectra. The absorption intensities of these three peaks for both M-N-A-S-H phases lie between those of the two M-A-S-H phases (Fig. 1d). The only exception is indicated by peak A of the M-N-A-S-H 0.8_0.1, which showed slightly higher absorption intensities compared to the M-A-S-H phases.

3.1.2 Comparison with natural phyllosilicates

The magnesium aluminium silicate hydrate phases with (M-N-A-S-H 0.8_0.1 and M-N-A-S-H 1.2_0.1) and without sodium (M-A-S-H 1.1_0.05 and M-A-S-H 1.1_0.1) had a similar edge position compared to the natural references (Fig. 2). Vermiculite, antigorite and periclase have distinct spectra as compared to the M-(N)-A-S-H phases (Fig. 2). In antigorite, the position of peak B was clearly shifted to higher energies and the shape of this same peak was asymmetrical with a light shoulder on the low energy side. In vermiculite, peaks A, B had lower absorption intensities and their position was shifted with respect to the M-(N)-A-S-H phases. Peak C had a shoulder on the high energy side of peak B. Periclase has a near-edge region with four peaks distinct from the investigated phases.

When comparing the experimental spectra with the Mg-Al phyllosilicate palygorskite it was observed that the latter has a pre-edge peak (before peak A) which was not detected in the M-(N)-A-S-H phases (Fig. 2, Table 2). Furthermore, the absorption intensity of peaks A, B and C was different from the M-(N)-A-S-H phases. In particular, peak C had a much lower absorption intensity than in the M-(N)-A-S-H phases (Table 2). Additionally, the absorption intensity of peak C was lower than peak A, as also observed for almost all montmorillonites (SWy2, STx1, Milos, Na-IFM) and illite. The only natural Mg-Al mixed phyllosilicates having comparable A, B and C peak shapes and indicating an absorption intensity of peak A lower than peak C, similar to the M-(N)-A-S-H phases, are clinochlore and montmorillonite SWy1 (Table 2). Furthermore, the difference between peak A and C is in SWy1 (0.04) much smaller, whereas the peak ratio of A/C in clinochlore (0.29) is more similar to the M-(N)-A-S-H phases (0.16 to 0.23).

Comparison with the Mg-phyllosilicate talc indicates a much higher absorption intensity for peaks A, B and C and a peak A to C relationship, which is the exact opposite to that of the M-(N)-A-S-H phases. Sepiolite shows a similar relationship between peaks A and C,

and it displays more similarities in the absorption intensity to the experimental phases. The brucite spectrum has a similar peak A and C relationship, a shoulder on the lower energy side of peak A is observed distinguishing it from the M-(N)-A-S-H phases.

Detailed observations of peaks D, E, F and G revealed that the intensities of peaks E and G are most similar to those in sepiolite whereas the intensity of peak F is comparable to both sepiolite and clinochlore (Fig. 3). Peak E is most equivalent to clinochlore in the case of the M-A-S-H phases, whereas the absorption intensity of both M-N-A-S-H phases is slightly lower compared to both references. Peak D is only present in brucite, talc, sepiolite and vermiculite, but the shape in all of these references differs from the M-(N)-A-S-H phases (Fig. 2).

Linear combination (LC) fits performed over the whole range of the spectra using all magnesium containing aluminum silicate hydrates and all natural references result in best fits with clinochlore and sepiolite. The results indicate a high percentage of clinochlore, with up to 70% for M-A-S-H 1.1_0.05 and M-N-A-S-H 0.8_0.1, 80% and 90 % for the and M-N-A-S-H 1.2_0.1 and M-A-S-H 1.1_0.1, respectively. In particular the M-A-S-H 1.1_0.1 phase, shows a good agreement between the fits and the experimental data (Fig. 4). Indeed, the M-A-S-H 1.1_0.1 as well as both M-N-A-S-H phases absorption intensities for peaks A, B and C are most similar to clinochlore, whereas M-A-S-H 1.1_0.05 shows, especially for peak B, higher intensities in the mid-range between clinochlore and sepiolite (Fig. 3a and b).

4. Discussion

4.1 . Comparison between M-S-H and M(N)-A-S-H phases

The M-(N)-A-S-H experimental spectra resemble those of the M-S-H spectrum, with the typical peaks A, B, C, D, E, F, and G, indicating the presence of a similar structures, i.e. a layering similarly to talc plus an interlayer containing Mg hydroxide similarly to brucite

as discussed in (Vespa et al., 2018). It has to be noted that peaks B and F indicate the first scattering neighbours O, Mg, Si (Fig. 5a) and further octahedral or tetrahedral cations which may be present, such as Al in the case of the M-(N)-A-S-H phases. Intensity changes of especially peak B are indicative of further cation incorporation in the Mg octahedral layer as demonstrated in Vespa et al., 2017; Vespa et al., 2018 for Ca uptake in the M-C-S-H. All other peaks reflect the multiple scattering of the cations and especially distal oxygens (Vespa et al., 2017; Vespa et al., 2018). Subsequently, changes of peaks B and F suggest a different coordination environment.

Investigations on M-S-H phases have shown that the position of the absorption edge (between the pre-edge and peak A) is indicative of octahedral coordinated Mg (Vespa et al., 2018). Furthermore, the ab initio XANES calculations have shown that peak B can be assigned to the Mg-O coordination up to ~2.6 Å and near neighbouring shells, i.e. Mg, Si up to ~3.2 Å (Fig. 5a). Moreover, the shape of this peak with a shoulder on the high energy side is indicative of two geometrically slightly distinct Mg sites in the structure and discussed in detail for the talc structure (Vespa et al., 2017; Vespa et al., 2018) (Fig. 1b and 5a).

The higher absorption intensities of peak B for the M-A-S-H 1.1_0.05 and both M-N-A-S-H phase compared to the M-S-H 1 (Fig. 1b) suggest a possible accommodation of Al in the structure as also observed and suggested for the mixed Mg-Ca silicate hydrates (Vespa et al., 2018). In fact, Al-NMR measurements (Bernard et al., 2020a) have confirmed that aluminum is taken up to a comparable extent both in the octahedral magnesium oxide as well as in the tetrahedral silicon oxide layer (Fig. 5a). Note that Al-NMR measurements have indicated that zeolitic precursors and a low amount of NO_3-hydrotalcite-like phases formed in addition to M-A-S-H in the M-N-A-S-H sample which contains $NaNO_3$ (Bernard et al., 2020a). However, the strong similarity of the spectra of

M-A-S-H and M-N-A-S-H observed here suggest that only little NO_3-hydrotalcite-like phase had formed in the investigated samples containing nitrate and aluminum.

The structural similarities between the M-N-A-S-H and the M-A-S-H do not suggest Na accommodation in the main-layer structure. This result is in good agreement with wet chemistry and NMR investigations of the same samples, where sodium has been found to be present mainly in the solution and to a limited extent as exchangeable cations on surface sites and not within the octahedral or tetrahedral layer (Bernard et al., 2019).

To summarise, both M-A-S-H and M-N-A-S-H phases exhibit a layered structure in which Mg is attached to oxygens in a manner similar to Mg coordination in talc and to hydroxide groups similarly to Mg coordination in the brucite structure. Furthermore, the results reveal that accommodation of aluminum is possible in both octahedral and tetrahedral positions, while sodium is most probably not incorporated within the structure.

4.2 Comparison between natural phyllosilicates and M-(N)-A-S-H phases

Comparison of M-N-A-S-H 0.8_0.1 and M-N-A-S-H 1.2_0.1 and M-A-S-H 1.1_0.05 and M-A-S-H 1.1_0.1 with natural containing Mg-Al silicate hydrate phases, i.e. phyllosilicates, is an important step in the further assessment of Al incorporation in these phases. Furthermore, this comparison may give additional information on crystallographic sites Al might occupy, i.e. octahedral and/or tetrahedral sites.

The spectral features of the M-(N)-A-S-H phases do not resemble the ones from antigorite, a phyllosilicate with an ordering of one tetrahedral (T) and one octahedral (O) layer, i.e. TO phyllosilicate, nor to talc, a TOT phyllosilicate. Nevertheless, in the past M-S-H phases with a Mg/Si >1 were reported to have a structural layering similar to a TO phyllosilicate, whereas Mg/Si ≤ 1 were compared to talc or suggested having a TOT O (talc plus brucite) layering (Nied et al., 2016; Pedone et al., 2017; Vespa et al., 2018) or

311 to be comparable to sepiolite (Brew and Glasser, 2005). The latter has a TOT structure
312 containing water molecules bridging between the octahedral sites and long octahedral
313 chains with eight Mg atoms (Sanchez del Rio et al., 2011). It has to be noted that
314 antigorite, talc and sepiolites are phyllosilicates containing only Mg (and no Al),
315 explaining the differences observed in the spectral features. The samples investigated in
316 this study have Mg/Si ratios from 0.8 to 1.2, but all XANES spectra are very similar. The
317 differences detected between the M-(N)-A-S-H experimental spectra and the references
318 antigorite and talc, especially the shape of peak B in antigorite, suggest that, in these
319 phases, neither a TO nor a pure TOT layering has formed. The similarity to the M-S-H
320 with Mg/Si ratio ≤1 as observed by Vespa and co-authors (Vespa et al., 2018) suggests
321 that M-(N)-A-S-H also has a structure with TOT O layering comparable to clinochlore
322 (Fig. 5b). The different results observed between this study with Mg/Si ratio >1 and
323 literature data could derive from Al incorporation into the structure, since in nature,
324 phyllosilicates with a TO structure are not known to contain Al, suggesting Al
325 accommodation by the M-(N)-A-S-H structure.
326 The observed differences in the absorption intensity of peak A being lower than peak C
327 in both M-A-S-H and M-N-A-S-H agree well with the absorption spectrum of clinochlore
328 (Fig. 5b). This is the only phyllosilicate showing this particular relationship between
329 peaks A and C (Table 2). Clinochlore is a Mg-Al mixed phyllosilicate with a TOT O
330 layering (Fig. 5b), in which the O layer contains $Mg(OH)_2$ groups, similarly to brucite. In
331 the clinochlore structure Al can be present in the tetrahedral and both octahedral sites
332 of the TOT and O layers containing Mg-hydroxide (McMurchy, 1934). The structure can
333 also accommodate considerable amounts of Fe, depending on the variety of the
334 clinochlore, and Fe always occupies octahedral sites.

Further similarities observed between the sepiolite and the M-(N)-A-S-H phases tends to indicate that in the latter, the octahedral chains are broken and in between water molecules may be present. Palygorskite (Chiari and Giustetto, 2003) has a very similar structure to sepiolite, but with less water molecules bridging between the octahedral sites and shorter octahedral chains, in which Al is also accommodated. Furthermore, it has a different symmetry: palygorskite is monoclinic, whereas sepiolite is orthorhombic, explaining also the differences in spectral features (e.g. pre-edge peak in palygorskite).

The above observations suggest that the structure of the M-(N)-A-S-H phases forms a TOT O, layering, comparable to clinochlore, in which the O interlayer is filled by Mg-hydroxide groups. This result is in good agreement with the finding of Vespa and co-workers in which the M-S-H phases with Mg/Si ratio ≤1 show close similarities to a combined talc-brucite structure mimicing the clinochlore structure (Vespa et al., 2018). In-between the octahedral chains of the M-(N)-A-S-H structure, water or OH groups might be present as bridging molecules as in the sepiolite structure. This is further supported by the linear combination fits of the experimental XANES spectra and all references, showing best result with mainly clinochlore and some sepiolite as model compounds.

Moreover, the formation of a TOT O layering with octahedral Mg bound to oxygen and OH groups, respectively, supports the notion of Al accommodation in the M-(N)-A-S-H structure. The latter hypothesis is supported by the increased absorption intensity of peak B compared to that in the M-S-H 1 phase, as also postulated for the M-C-S-H by (Vespa et al., 2018). The crystallographic position of Al cannot be unambiguously indicated from the presently available data. A comparison with the reference clinochlore suggests that Al may be incorporated in both octahedral and tetrahedral sites, while

occupancy may be different. The current proposal of Al coordination in M-S-H phases is in good agreement with the Al NMR data reported by Bernard et al. (2020a).

5. Conclusions

The present study shows that state-of-the-art Mg K-edge XANES can be employed to characterise the poorly ordered structure of the M-A-S-H and M-N-A-S-H phases and, thus, improve our understanding of the accommodation of cations by these structures. The XANES results suggest that M-(N)-A-S-H phases have a TOT O layering, similarly to clinochlore, with water or OH groups bridging between the octahedral broken chains as in the sepiolite structure. Furthermore, the results suggest that Al may be accommodated in both octahedral and tetrahedral sites while the extent of occupancy may be different. The evidence is that Na is neither bonded in the octahedral nor the tetrahedral layer.

The results acquired from this study improve the long-term assessment of the geochemical evolution of interfaces between cement and clayey host rock in a geological repository, indicating the need to also consider M-S-H phases with Al incorporation.

Acknowledgments

The Geological Institute (Bern University) is thanked for providing the natural antigorite and clinochlore reference materials. Ellina Bernard is thanked for helpful discussions and for the preparation of the samples. The Paul Scherrer Institute (PSI, Villigen, Switzerland) is acknowledged for provision of synchrotron radiation beamtime at the Phoenix beamline of the Swiss Light Source (SLS) and the beamline scientists Dr. Cinthia

Piamonteze and Dr. Jan Dreiser for support during the optical set-up and operation of the X-Treme branchline. Financial support was provided by the CI Experiment belonging to the Mont Terri Consortium, Swisstopo.

References

Bernard, E., Dauzères, A., Lothenbach, B., 2018a. Magnesium and calcium silicate hydrates, Part II: Mg-exchange at the interface “low-pH” cement and magnesium environment studied in a C-S-H and M-S-H model system. Applied Geochemistry 89, 210-218.

Bernard, E., Lothenbach, B., Cau-Dit-Coumes, C., Chlique, C., Dauzères, A., Pochard, I., 2018b. Magnesium and calcium silicate hydrates, Part I: Investigation of the possible magnesium incorporation in calcium silicate hydrate (C-S-H) and of the calcium in magnesium silicate hydrate (M-S-H). Applied Geochemistry 89, 229-242.

Bernard, E., Lothenbach, B., Cau-dit-Coumes, C., Pochard, I., Rentsch, D., 2020a. Aluminium uptake in magnesium silicate hydrates. Cement and Concrete Research 128, 105931.

Bernard, E., Lothenbach, B., Le Goff, F., Pochard, I., Dauzères, A., 2017. Effect of magnesium on calcium silicate hydrates (C-S-H). Cement and Concrete Research 97, 61-72.

Bernard, E., Lothenbach, B., Pochard, I., Cau-dit-Coumes, C., 2019. Alkali binding by magnesium silicate hydrates. Journal of the American Ceramic Society 102, 6322–6336.

Bernard, E., Lothenbach, B., Rentsch, D., 2020b. Formation of magnesium (aluminum)-silicate hydrates in the MgO-NaO_2-Al_2O_3-SiO_2-H_2O system. Materials & Design submitted.

Brew, D.R.M., Glasser, F.P., 2005. Synthesis and characterisation of magnesium silicate hydrate gels. Cement and Concrete Research 35, 85-98.

Chiari, G., Giustetto, R.R., G., 2003. Crystal structure refinements of palygorskite and Maya Blue from molecular
modelling and powder synchrotron diffraction. European Journal of Mineralogy 15, 21-33.

Dauzères, A., Achiedo, G., Nied, D., Bernard, E., Alahrache, S., Lothenbach, B., 2016. Magnesium perturbation in low-pH concretes placed in clayey environment—solid characterizations and modeling. Cement and Concrete Research 79, 137-150.

Fernandez, L., Alonso, C., Andrade, C., Hidalgo, A., 2008. The interaction of magnesium in hydration of C3S and CSH formation using 29Si MAS-NMR. Journal of Materials Science 43, 5772-5783.

Flank, A.M., Cauchon, G., Lagarde, P., Bac, S., Janousch, M., Wetter, R., Dubuisson, J.M., Idir, M., Langlois, F., Moreno, T., Vantelon, D., 2006. LUCIA, a microfocus soft XAS beamline. Nuclear Instruments and Methods in Physics Research Section B: Beam Interactions with Materials and Atoms 246, 269-274.

Gruner, J.W., 1934. The crystal structures of talc and pyrophyllite. Zeitschrift fuer Kristallographie, Kristallgeometrie, Kristallphysik, Kristallchemie 88, 412-419.

Jenni, A., Mäder, U., Lerouge, C., Gaboreau, S., Schwyn, B., 2014. In situ interaction between different concretes and Opalinus Clay. Physics and Chemistry of the Earth, Parts A/B/C 70–71, 71-83.

Lothenbach, B., Nied, D., L'Hôpital, E., Achiedo, G., Dauzères, A., 2015. Magnesium and calcium silicate hydrates. Cement and Concrete Research 77, 60-68.

Mäder, U., Jenni, A., Lerouge, C., Gaboreau, S., Miyoshi, S., Kimura, Y., Cloet, V., Fukaya, M., Claret, F., Otake, T., Shibata, M., Lothenbach, B., 2017. 5-year chemico-physical evolution of concrete–claystone interfaces, Mont Terri rock laboratory (Switzerland). Swiss Journal of Geosciences 110, 307-327.

McMurchy, G.C., 1934. The Crystal Structure of the Chlorite Minerals. Zeitschrift fuer Kristallographie, Kristallgeometrie, Kristallphysik, Kristallchemie (-144,1977) 88, 420 - 432.

McMurchy, G.C., 1977. The crystal structure of the chlorite minerals. Zeitschrift fuer Kristallographie, Kristallgeometrie, Kristallphysik, Kristallchemie 144.

Newville, M., 2001. IFFEFFIT: interactive XAFS analysis and FEFF fitting. Journal of Synchrotron Radiation 8, 322-324.

Nied, D., Enemark-Rasmussen, K., L'Hopital, E., Skibsted, J., Lothenbach, B., 2016. Properties of magnesium silicate hydrates (M-S-H). Cement and Concrete Research 79, 323-332.

Pedone, A., Palazzetti, F., Barone, V., 2017. Models of Aged Magnesium–Silicate–Hydrate Cements Based on the Lizardite and Talc Crystals: A Periodic DFT-GIPAW Investigation. The Journal of Physical Chemistry C 121, 7319-7330.

Piamonteze, C., Flechsig, U., Rusponi, S., Dreiser, J., Heidler, J., Schmidt, M., Wetter, R., Calvi, M., Schmidt, T., Pruchova, H., Krempasky, J., Quitmann, C., Brune, H., Nolting, F., 2012. X-Treme beamline at SLS: X-ray magnetic circular and linear dichroism at high field and low temperature. Journal of Synchrotron Radiation 19, 661-674.

Poinssot, C., Baeyens, B., Bradbury, M.H., 1999. Experimental and modelling studies of caesium sorption on illite. Geochimica et Cosmochimica Acta 63, 3217-3227.

Pytel, Z., Malolepszy, J., 2000. DTA studies of phases synthesized in the system CaO–MgO–SiO_2–H_2O. Silicate Industrials 65, 81-85.

Ravel, B., Newville, M., 2005. ATHENA, ARTEMIS, HEPHAESTUS: data analysis for X-ray absorption spectroscopy using IFEFFIT. Journal of Synchrotron Radiation 12, 537-541.

Richardson, I.G., 2008. The calcium silicate hydrates. Cement and Concrete Research 38, 137-158.

Roosz, C., Grangeon, S., Blanc, P., Montouillout, V., Lothenbach, B., Henocq, P., Giffaut, E., Vieillard, P., Gaboreau, S., 2015. Crystal structure of magnesium silicate hydrates (M-S-H): The relation with 2:1 Mg–Si phyllosilicates. Cement and Concrete Research 73, 228-237.

Sanchez del Rio, M., Garcia-Romero, E., Suarez, M., da Silva, I., Fuentes-Montero, L., Martinez-Criado, G., 2011. ariability in sepiolite: diffraction studies. American Mineralogist 96, 1443-1454.

Shrivastava, O.P., Komarneni, S., Breval, E., 1991. Mg2+ uptake by synthetic tobermorite and xonotlite. Cement and Concrete Research 21, 83-90.

Vespa, M., Dähn, R., Huthwelker, T., Wieland, E., 2017. Soft X-ray absorption near-edge investigations of Mg-containing mineral phases relevant for cementitious materials. Physics and Chemistry of the Earth, Parts A/B/C 99, 168-174.

Vespa, M., Lothenbach, B., Dähn, R., Huthwelker, T., Wieland, E., 2018. Characterisation of magnesium silicate hydrate phases (M-S-H): A combined approach using synchrotron-based absorption-spectroscopy and ab initio calculations. Cement and Concrete Research 109, 175-183.

Figure captions

Fig. 1. Different representations of normalized X-ray absorption near-edge spectra at the Mg K-edge of various M-S-H, M-A-S-H and M-N-A-S-H.

Fig. 2. Normalized X-ray absorption near-edge spectra at the Mg K-edge of natural minerals. The reference lines A to G indicate the energy position of structural features of M-S-H 1 compared to the natural minerals as well as M-A-S-H and M-N-A-S-H phases. Palig. = palygorskite, for further details see table 1.

Fig. 3. Normalized X-ray absorption near-edge spectra at the Mg K-edge of sepiolite, clinochlore and various M-A-S-H and M-N-A-S-H.

Fig. 4. Linear combination fits of a) M-A-S-H 1.1_0.05, b) M-A-S-H 1.1_0.1, c) M-N-A-S-H 0.8_0.1, and c) M-N-A-S-H 1.2_0.1.

Fig. 5. a) The model of the Talc structural (Gruner, 1934); b) the model of the clinochlore structure (McMurchy, 1977). T= tetrahedral and O= octahedral layers. Numbers show distances between atoms in Å. Red atoms=oxygen, green and brown octahedra=Mg atoms (M1 and M2 crystallographic sites) and blue tetrahedra= Si atoms.

498 **Table 1.** List of natural minerals used in this study (Poinssot et al., 1999)

Mineral Names	Chemcal Formula	origin / source	reference
Periclase	MgO	Sigma-Aldrich	-
Brucite	$Mg(OH)_2$	Sigma-Aldrich	-
Talc	$Mg_3Si_4O_{10}(OH)_2$	Alfa-Aeser	-
Antigorite	$Mg_3Si_2O_5(OH)_4$	Geisspfad, Binntal (CH) / Uni. Bern	-
Clinochlore	$[Mg_{1.90}Al_{1.24}Fe_{2.86}]_6[Si_{2.78}Al_{1.22}]_4O_{10}(OH)_8$	Gerstenegg, Grimsel (CH) / Uni. Bern	-
Palygorskite	$(Mg_{0.33}Ca_{0.62}Na_{0.04}K_{0.13})[Al_{1.50}Fe(III)_{0.52}$ $Fe(II)_{0.01}Mn_{0.01}Mg_{1.91}Ti_{0.06}]$ $[Si_{7.88}Al_{0.22}]O_{20}(OH)_4$	Gadsden County, Florida, (USA) / CMS, CM	-
Sepiolite	$(K_{0.01})[Mg_{5.54}Al_{0.35}Mn_{0.02}Fe(II)_{0.04}Fe(III)_{0.14}]$ $[Si_{7.90}Al_{0.1}]O_{20}(OH)_4$	Valdemore (Spain) / CMS, CM	-
Vermiculite	$(Mg_{2.27}Ca_{2.92}K_{0.01})[Mg_{5.98}Mn_{0.01}Ti_{0.01}]$ $[Si_{7.71}Al_{0.13}Fe^{(III)}{}_{0.16}]O_{20}(OH)_4$	Llano, Texas (USA) / CMS, CM	-
Illite	$[Si_{7.04}Al_{0.96}][Al_{2.34}Fe(III)_{0.98}Mg_{0.66}]$ $(Ca_{0.08}Na_{0.24}K_{1.28})O_{20}(OH)_4$	PSI-LES courtesy of Dr. Bart Baeyens	[1,2]
Texas (STx-1)	$[Si_{7.91}Al_{0.09}]$ $[Al_{3.12}Fe(III)_{0.10}Mg_{0.79}]$ $Na_{0.88}O_{20}(OH)_4$	PSI-LES courtesy of Dr. Bart Baeyens	[2]
Wyoming-1 (SWy-1)	$[Si_{7.73}Al_{0.27}]$ $[Al_{3.06}Mg_{0.46}FeII_{0.03}FeIII_{0.44}]O_{20}(OH)_4$	PSI-LES courtesy of Dr. Bart Baeyens	[2]
Wyoming-2 (SWy-2)	$[Si_{7.74}Al_{0.26}][Al_{3.06}Mg_{0.48}FeII_{0.03}\,FeIII_{0.42}]$ $Na_{0.77}O_{20}(OH)_4$	PSI-LES courtesy of Dr. Bart Baeyens	[2]
Milos	$[Si_{7.76}Al_{0.24}][Al_{3.0}Fe(II)_{0.02}Fe(III)_{0.44}\,Mg_{0.54}]$ $Na_{0.79}O_{20}(OH)_4$	PSI-LES courtesy of Dr. Bart Baeyens	[2]
Na iron-free montmorillonite (Na-IFM)	$Na_{0.28}[Si_{7.91}Al_{0.09}][Al_{3.13}\,Mg_{0.87}]$ $F_4]O_{20}(OH)_4$	PSI-LES courtesy of Dr. Bart Baeyens	[3 & references therein]

Illite, Texas, Wyoming 1 and 2, and Milos are all montmorillonites;ement Laboratory

Uni. Bern: University of Bern, Geological Instiute,CMS, CM: Clay Mineral Society, Clay Minerals, PSI-LES: Paul Scherrer Institute, Waste Management

499 References: 1= Poinssot et al., 1999; 2= Vantelon et al., 2003; Soltermann et al., 2013

500

501

502 **Table 2.** Indication of the absorption intensities of peaks A and C as well as the presence of the pre-edge feature and the Mg/Si relationship in the
503 different experimental samples and reference materials

Sample	Mg/Si	pre-edge	A	C	A/C
M-S-H 1	1.00		1.79	1.85	0.96756757
M-A-S-H 1.1_0.05	1.10	-	1.81	2.04	0.8872549
M-A-S-H 1.1_0.1	1.10	-	1.72	1.90	0.90526316
M-N-A-S-H 0.8_0.1	0.80	-	1.85	2.01	0.92039801
M-N-A-S-H 1.2_0.1	1.20	-	1.76	1.97	0.89340102
Talc	0.75	-	3.67	2.81	1.30604982
Antigorite	1.50	-	1.77	2.23	0.79372197
Sepiolite	0.70	-	2.30	2.09	1.10047847
Illite	0.09	-	2.27	2.13	1.0657277
Wyoming-2	0.06	-	1.87	1.80	1.03888889
Wyoming-1	0.06	-	1.93	1.97	0.97969543
Milos	0.10	-	1.83	1.72	1.06395349
Texas-1	0.10		1.85	1.75	1.05714286
Na-IFM	0.11	-	1.82	1.70	1.07058824
Clinochlore	0.68	-	1.71	2.00	0.855
Palygorskite	0.04	yes	1.73	1.57	1.10191083
Brucite	0.00	-	1.41	1.55	0.90967742
Periclase	0.00	-	2.03	2.11	0.96208531
Vermiculite	1.07	-	1.65	-	-
A and C indicate Peak A and C, respectively					
Na-IFM: Na Iron-Free Montmorillonite					

504
505

Figures

Fig. 1

a)

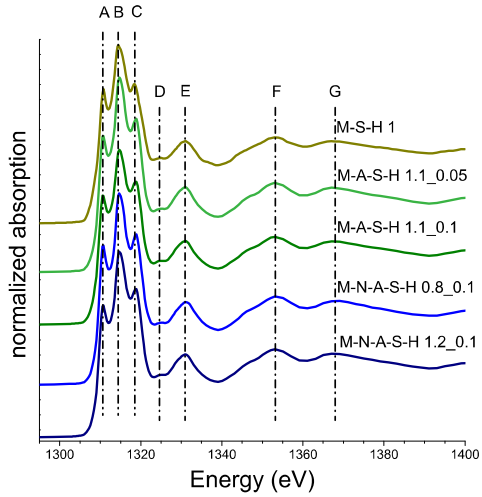

b)

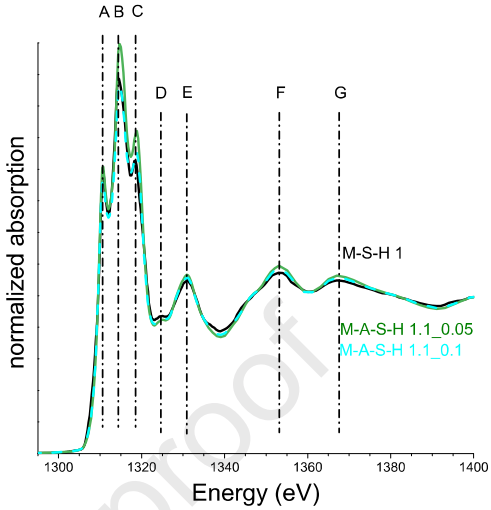

c)

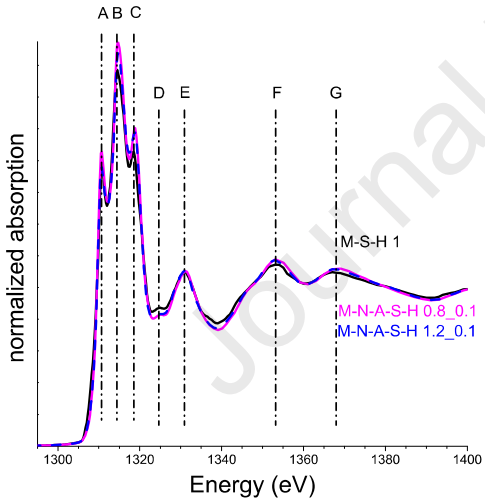

d)

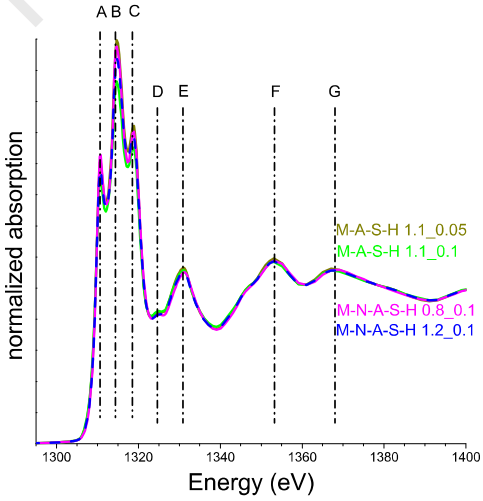

Fig. 2

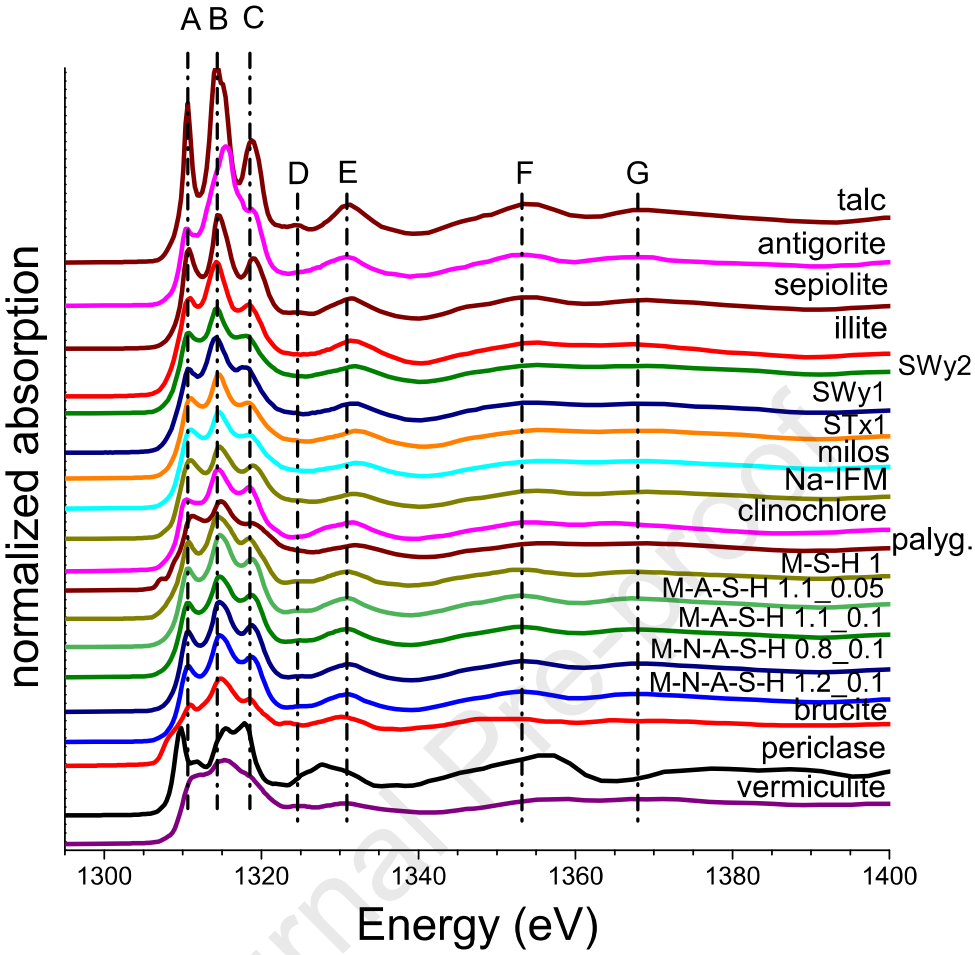

Fig. 3

a)

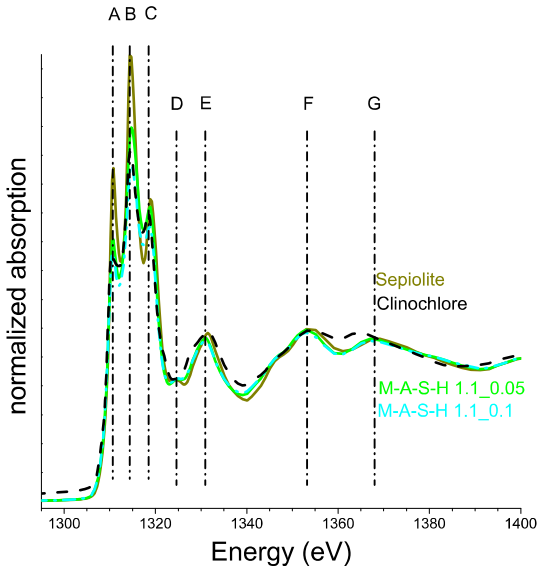

b)

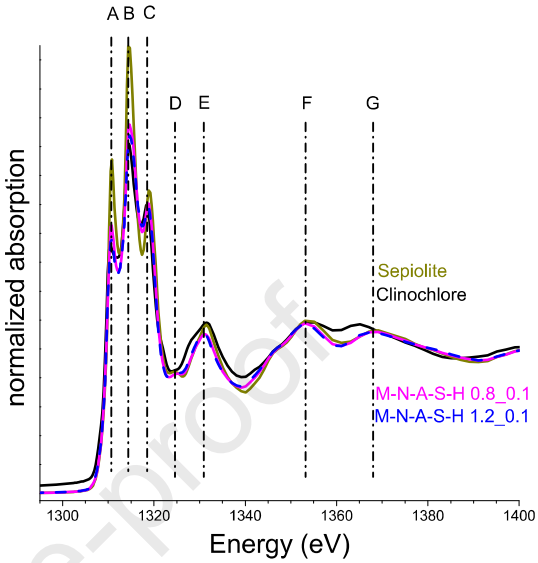

Fig. 4

a)

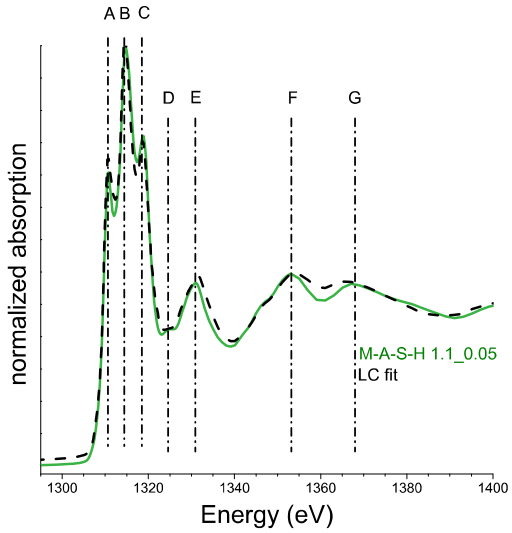

b)

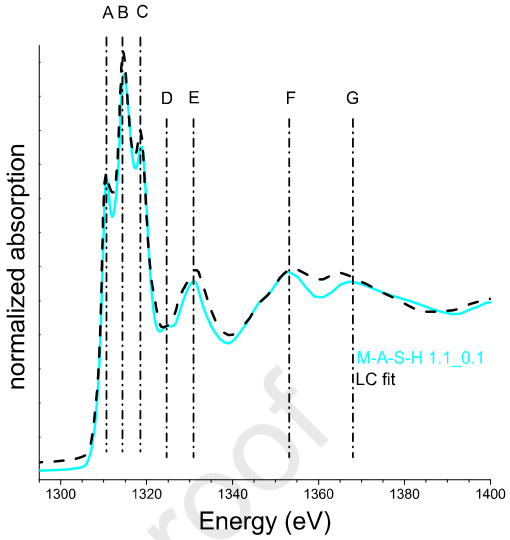

c)

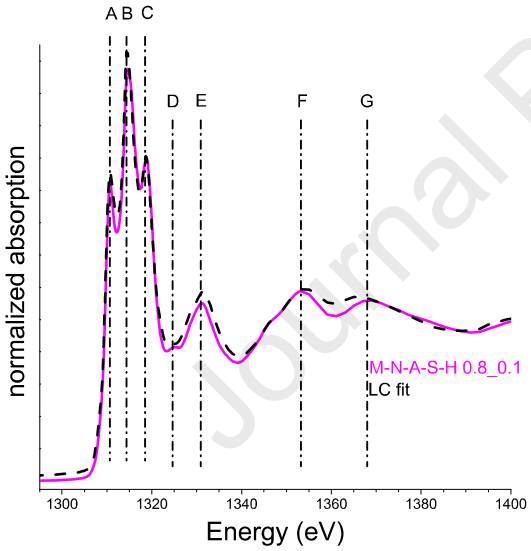

d)

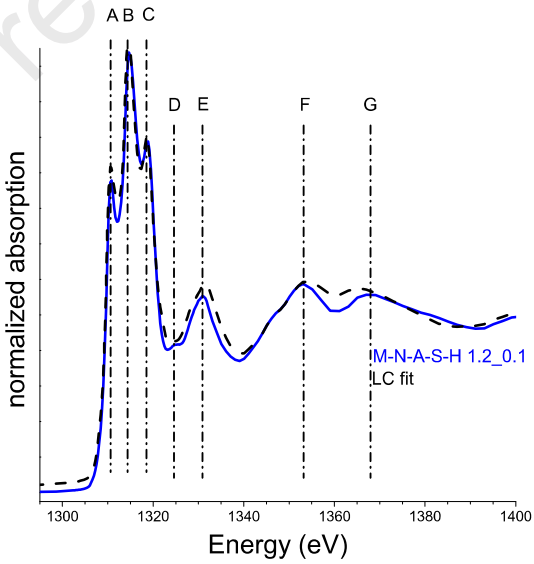

Fig. 5

a)

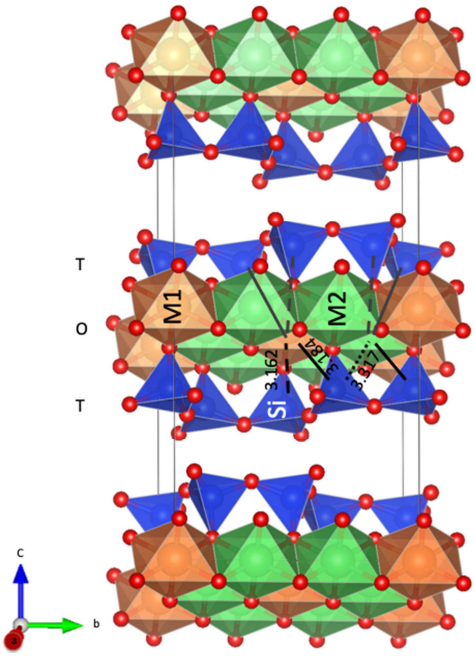

b)

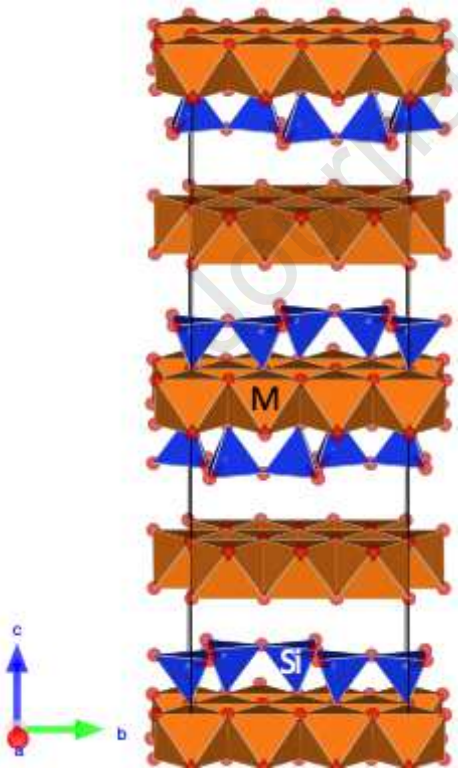

Mineral Names	Chemcial Formula	origin / source	reference
Periclase	MgO	Sigma-Aldrich	-
Brucite	$Mg(OH)_2$	Sigma-Aldrich	-
Talc	$Mg_3Si_4O_{10}(OH)_2$	Alfa-Aeser	-
Antigorite	$Mg_3Si_2O_5(OH)_4$	Geisspfad, Binntal (CH) / Uni. Bern	-
Clinochlore	$[Mg_{1.90}Al_{1.24}Fe_{2.86}]_6[Si_{2.78}Al_{1.22}]_4O_{10}(OH)_8$	Gerstenegg, Grimsel (CH) / Uni. Ber	-
Palygorskite	$_{0.04}K_{0.13})[Al_{1.50}Fe(III)_{0.52}Fe(II)_{0.01}Mn_{0.01}Mg_{1.91}Ti_{0.06}][Si_{7.88}$	den County, Florida, (USA) / CMS	-
Sepiolite	$_{01})[Mg_{5.54}Al_{0.35}Mn_{0.02}Fe(II)_{0.04}Fe(III)_{0.14}][Si_{7.90}Al_{0.1}]O_{20}($	Valdemore (Spain) / CMS, CM	-
Vermiculite	$_{27}Ca_{2.92}K_{0.01})[Mg_{5.98}Mn_{0.01}Ti_{0.01}][Si_{7.71}Al_{0.13}Fe^{(III)}_{0.16}]O_{20}$	Llano, Texas (USA) / CMS, CM	-
Illite	$_{7.04}Al_{0.96}][Al_{2.34}Fe(III)_{0.98}Mg_{0.66}](Ca_{0.08}Na_{0.24}K_{1.28})O_{20}(OH$	PSI-LES courtesy of Dr. Bart Baeyer	[5,6]
Texas (STx-1)	$[Si_{7.91}Al_{0.09}][Al_{3.12}Fe(III)_{0.10}Mg_{0.79}]Na_{0.88}O_{20}(OH)_4$	PSI-LES courtesy of Dr. Bart Baeyer	[6]
Wyoming-1 (SWy-1)	$Si_{7.73}Al_{0.27}][Al_{3.06}Mg_{0.46}FeII_{0.03}FeIII_{0.44}]O_{20}(OH)_4$	PSI-LES courtesy of Dr. Bart Baeyer	[6]
Wyoming-2 (SWy-2)	$[Si_{7.74}Al_{0.26}][Al_{3.06}Mg_{0.48}FeII_{0.03}FeIII_{0.42}]Na_{0.77}O_{20}(OH)_4$	PSI-LES courtesy of Dr. Bart Baeyer	[6]
Milos	$Si_{7.76}Al_{0.24}][Al_{3.0}Fe(II)_{0.02}Fe(III)_{0.44}Mg_{0.54}]Na_{0.79}O_{20}(OH)$	PSI-LES courtesy of Dr. Bart Baeyer	[6]
Na iron-free montmorillonite (Na-IFM	$Na_{0.28}[Si_{7.91}Al_{0.09}][Al_{3.13}Mg_{0.87}F_4]O_{20}(OH)_4$	PSI-LES courtesy of Dr. Bart Baeyer	[7 and references therein]

Illite, Texas, Wyoming 1 and 2, and Milos are all montmorillonites;ement Laboratory

Uni. Bern: University of Bern, Geological Instiute,CMS, CM: Clay Mineral Society, Clay Minerals, PSI-LES: Paul Scherrer Institute, Waste Management

Mineral Names	**Chemcal Formula**	**origin / source**	**reference**
Periclase	MgO	Sigma-Aldrich	-
Brucite	$Mg(OH)_2$	Sigma-Aldrich	-
Talc	$Mg_3Si_4O_{10}(OH)_2$	Alfa-Aeser	-
Antigorite	$Mg_3Si_2O_5(OH)_4$	Geisspfad, Binntal (CH) / Uni. Bern	-
Clinochlore	$[Mg_{1.90}Al_{1.24}Fe_{2.86}]_6[Si_{2.78}Al_{1.22}]_4O_{10}(OH)_8$	Gerstenegg, Grimsel (CH) / Uni. Bern	-
Palygorskite	$(Mg_{0.33}Ca_{0.62}Na_{0.04}K_{0.13})[Al_{1.50}Fe(III)_{0.52}$ $Fe(II)_{0.01}Mn_{0.01}Mg_{1.91}Ti_{0.06}]$ $[Si_{7.88}Al_{0.22}]O_{20}(OH)_4$	Gadsden County, Florida, (USA) / CMS, CM	-
Sepiolite	$(K_{0.01})[Mg_{5.54}Al_{0.35}Mn_{0.02}Fe(II)_{0.04}Fe(III)_{0.14}]$ $[Si_{7.90}Al_{0.1}]O_{20}(OH)_4$	Valdemore (Spain) / CMS, CM	-
Vermiculite	$(Mg_{2.27}Ca_{2.92}K_{0.01})[Mg_{5.98}Mn_{0.01}Ti_{0.01}]$ $[Si_{7.71}Al_{0.13}Fe^{(III)}_{0.16}]O_{20}(OH)_4$	Llano, Texas (USA) / CMS, CM	-
Illite	$[Si_{7.04}Al_{0.96}][Al_{2.34}Fe(III)_{0.98}Mg_{0.66}]$ $(Ca_{0.08}Na_{0.24}K_{1.28})O_{20}(OH)_4$	PSI-LES courtesy of Dr. Bart Baeyens	[1,2]
Texas (STx-1)	$[Si_{7.91}Al_{0.09}][Al_{3.12}Fe(III)_{0.10}Mg_{0.79}]$ $Na_{0.88}O_{20}(OH)_4$	PSI-LES courtesy of Dr. Bart Baeyens	[2]
Wyoming-1 (SWy-1)	$[Si_{7.73}Al_{0.27}]$ $[Al_{3.06}Mg_{0.46}FeII_{0.03}FeIII_{0.44}]O_{20}(OH)_4$	PSI-LES courtesy of Dr. Bart Baeyens	[2]
Wyoming-2 (SWy-2)	$[Si_{7.74}Al_{0.26}][Al_{3.06}Mg_{0.48}FeII_{0.03}FeIII_{0.42}]$ $Na_{0.77}O_{20}(OH)_4$	PSI-LES courtesy of Dr. Bart Baeyens	[2]
Milos	$[Si_{7.76}Al_{0.24}][Al_{3.0}Fe(II)_{0.02}Fe(III)_{0.44}Mg_{0.54}]$ $Na_{0.79}O_{20}(OH)_4$	PSI-LES courtesy of Dr. Bart Baeyens	[2]
Na iron-free montmorillonite (Na-IFM)	$Na_{0.28}[Si_{7.91}Al_{0.09}][Al_{3.13}Mg_{0.87}]$ $F_4]O_{20}(OH)_4$	PSI-LES courtesy of Dr. Bart Baeyens	[3 & references therein]

Illite, Texas, Wyoming 1 and 2, and Milos are all montmorillonites;ement Laboratory

Uni. Bern: University of Bern, Geological Instiute,CMS, CM: Clay Mineral Society, Clay Minerals, PSI-LES: Paul Scherrer Institute, Waste Management

References: 1= Poinssot et al., 1999; 2= Vantelon et al., 2003; Soltermann et al., 2013

cotron option return

sample	A	B	C	D	E	F	G	x	y
signal	NB	NB	NB/MS	MS	MS	MS	MS		
M-A-S-H 1	1311	1315	1319	1325	1331	1353	1367		
M-A-S-H 2	1311	1315	1319	1325	1331	1352	1367		
M-N-A-S-H 3	1311	1315	1319	1325	1331	1352	1368		
M-N-A-S-H 4	1311	1315	1319	1325	1331	1353	1367		
Talc	1311	1314	1319	1324	1331	1353	1368		
Antigorite	1311	1315	1319	-	1331	1353	1367		
Sepiolite	1311	1314	1319	1325	1331	1353	1369		
Illite	1311	1314	1318	-	1331	1355	1367		
SWy2	1311	1314	1318	-	1332	1355	1368		
SWy1	1311	1314	1318	-	1332	1354	1367		
Milos	1311	1315	1318	-	1332	1355	1369		
Syn.Mtm Fe free	1311	1315	1319	1325	1332	1355	1369		
Clinichlore	1311	1315	1319	1325	1331	1353	1369		
Palygorkite	1311	1315	1319	-	1332	1355	1369		
Brucite	1311	1315	1318	1323	1330	1353	1364		
Periclase	1310	1316	1319	-	1329	1357	1380		
Vermiculite	1312	1315	-	1325	1331	1357	1367		

NB &MS indicate nearest neighbours and multiple scattering; x & y indicate A/C and B/x peak absorption ratio

sample	pre-ede	A	B	C	D	E	F	G	A/C=x	B/x=y	B/A	B/C	F/G
signal		NB	NB	NB/MS	MS	MS	MS	MS					
M-A-S-H 1	-	1.81	2.59	2.04	0.84	1.13	1.19	1.12	0.89	2.92	1.43	1.27	1.06
M-A-S-H 2	-	1.72	2.32	1.90	0.85	1.11	1.17	1.11	0.91	2.56	1.35	1.22	1.05
M-N-A-S-H 3	-	1.85	2.55	2.01	0.83	1.11	1.17	1.12	0.92	2.77	1.38	1.27	1.04
M-N-A-S-H 4	-	1.76	2.47	1.97	0.83	1.10	1.17	1.11	0.89	2.76	1.40	1.25	1.05
Talc	-	3.67	4.56	2.81	0.85	1.33	1.35	1.21	1.31	3.49	1.24	1.62	1.12
Antigorite	-	1.77	3.67	2.23	-	1.12	1.17	1.13	0.79	4.62	2.07	1.65	1.04
Sepiolite	-	2.30	3.08	2.09	0.84	1.17	1.20	1.12	1.10	2.80	1.34	1.47	1.07
Illite	-	2.27	3.10	2.13	-	1.28	1.25	1.20	1.07	2.91	1.37	1.46	1.04
SWy2	-	1.87	2.43	1.80	-	1.10	1.12	1.10	1.04	2.34	1.30	1.35	1.02
SWy1	-	1.93	2.65	1.97	-	1.13	1.15	1.13	0.98	2.70	1.37	1.35	1.02
Milos	-	1.83	2.24	1.72	-	1.06	1.10	1.10	1.06	2.11	1.22	1.30	1.00
Syn.Mtm Fe free	-	1.82	2.13	1.70	0.90	1.05	1.11	1.09	1.07	1.99	1.17	1.25	1.02
Clinichlore	-	2.32	3.09	2.13	0.84	1.17	1.19	1.13	1.09	2.84	1.33	1.45	1.05
Palygorskite	yes	1.73	2.07	1.57	-	1.06	1.10	1.10	1.10	1.88	1.20	1.32	1.00

Brucite	-	1.41	2.02	1.55	1.00	1.13	1.09	1.05	0.91	2.22	1.43	1.30	1.04
Periclase	-	2.03	2.02	2.11	-	1.27	1.47	1.1	0.96	2.10	1.00	0.96	1.34
Vermiculite	-	1.65	1.98	-	0.93	0.99	1.08	1.09	-	-	1.20	-	0.99

NB &MS indicate nearest neighbours and multiple scattering; x & y indicate A/C and B/x peak absorption ratio

data read from backgrouns substracted and normalised spectra at the maximum of each peak

Sample	Mg/Si	pre-edge	A	C	A/C
M-S-H 1	1.00		1.79	1.85	0.96756757
M-A-S-H 1.1_0.05	1.10	-	1.81	2.04	0.8872549
M-A-S-H 1.1_0.1	1.10	-	1.72	1.90	0.90526316
M-N-A-S-H 0.8_0.1	0.80	-	1.85	2.01	0.92039801
M-N-A-S-H 1.2_0.1	1.20	-	1.76	1.97	0.89340102
Talc	0.75	-	3.67	2.81	1.30604982
Antigorite	1.50	-	1.77	2.23	0.79372197
Sepiolite	0.70	-	2.30	2.09	1.10047847
Illite	0.09	-	2.27	2.13	1.0657277
Wyoming-2	0.06	-	1.87	1.80	1.03888889
Wyoming-1	0.06	-	1.93	1.97	0.97969543
Milos	0.10	-	1.83	1.72	1.06395349
Texas-1	0.10		1.85	1.75	1.05714286
Na-IFM	0.11	-	1.82	1.70	1.07058824
Clinochlore	0.68	-	1.71	2.00	0.855
Palygorskite	0.04	yes	1.73	1.57	1.10191083
Brucite	0.00	-	1.41	1.55	0.90967742
Periclase	0.00	-	2.03	2.11	0.96208531
Vermiculite	1.07	-	1.65	-	-

A and C indicate Peak A and C, respectively

Na-IFM: Na Iron-Free Montmorillonite

Highlights should be submitted in a separate editable file in the online submission system. Please use 'Highlights' in the file name and include 3 to 5 bullet points (maximum 85 characters, including spaces, per bullet point).

Highlights to

- First Al-containing M-S-H synchrotron-based x-ray absorption near-edge spectroscopic data
- Al incorporation in the M-S-H structure is possible
- M-(N)-A-S-H structure is most similar to the clinochlore structure

Declaration of interests

☒ The authors declare that they have no known competing financial interests or personal relationships that could have appeared to influence the work reported in this paper.

Declarations of interest: none

☐The authors declare the following financial interests/personal relationships which may be considered as potential competing interests: